Communications in Physics, Vol. 33, No. 3 (2023), pp. 263-272
DOI: https://doi.org/10.15625/0868-3166/18218

Asymmetric tunneling of holes through a semiconductor junction in an arbitrary magnetization configuration

Loan T. Nguyen[1,2], **Haidang Phan**[2,4] **and Hoai T. L Nguyen**[2,3,†]

[1]*Hong Duc University, 565 Quang Trung road, Dong Ve, Thanh Hoa, Vietnam*
[2]*Graduate University of Science and Technology, 18 Hoang Quoc Viet, Cau Giay, Hanoi, Vietnam*
[3]*Institute of Physics, Vietnam Academy of Science and Technology, 10 Dao Tan, Ba Dinh, Hanoi, Vietnam*
[4]*Faculty of Civil Engineering, VNU University of Engineering and Technology, Hanoi, Vietnam*

E-mail: †nlhoai@iop.vast.vn

Received 4 April 2023
Accepted for publication 26 May 2023
Published 10 August 2023

Abstract. *In this paper, we investigate the asymmetry of hole tunneling through a magnetic semiconductor tunnel junction (GaMnAs/GaAs/GaMnAs) in general cases, where the magnetizations of the two electrodes are noncollinear and their magnitudes are not equal. The six-band* ***k.p*** *Hamiltonian is employed to describe the holes in the GaAs and GaMnAs layers, taking into account both spin-orbit and exchange interactions. Multi-band transfer-matrix formalism is applied to solve the Schrödinger equations for hole wave functions and derive the transmission coefficients. We investigate the transmission asymmetry as a function of both the magnetization magnitude at the right electrode and the angles between two magnetization vectors. The results provide better understanding about the dynamics of the anomalous tunneling Hall current during the magnetization switching process, which is important for designing and measuring spintronic devices.*

Keywords: spin-orbit interaction, III-V semiconductor, magnetic tunnel junction, multi-band transport, transfer matrix, k.p method.

Classification numbers: 85.75.-d, 75.76.+j,71.15.Ap.

1. Introduction

Spintronics is an exciting scientific field that investigates the use of the carriers' spin degrees of freedom to enhance the efficiency of electronic devices. Remarkable advances include magnetic

random-access memory (MRAM) and spin-transfer torque magnetic random-access memory (STT-MRAM) [1,2]. These devices were developed based on the discoveries of Giant Magnetoresistance (GMR), Tunnel Magnetoresistance (TMR), and Spin Transfer Torque (STT) [3–6], which rely on the mechanism of exchange interactions in magnetic materials.

In the last few decades, research in a new subfield of spintronics, called spinorbitronics, has gained considerable attention. This research branch focuses on exploiting quantum effects resulting from the interaction between the spin and its orbital trajectory (SOI) in spintronic systems. SOI-driven effects, such as the well-known Spin Hall effect and its inverse [7], promise the potential to develop a new generation of spintronic components and spin sensors that do not require magnetic fields.

Semiconductor systems are particularly intriguing among all spinorbitronic materials due to their potential for integrating into the existing electronics industry, as well as the numerous spin-orbit interaction mechanisms they exhibit. Among the semiconductor systems, extensive research has been conducted on GaAs semiconductors and their heterostructures. The combination of spin-orbit interaction with the crystal and structural asymmetry in these systems leads to several important effects, including spin galvanic [8], spin filtering [9], and spin rotation [10]. In compounds such as GaMnAs, the presence of both exchange and spin-orbit interactions is crucial for the discovery of a new category of effects known as the Tunneling Anomalous Hall Effect (TAHE) [11] or Anomalous Tunnel Hall Effect (ATHE) [12]. The latter was discovered by our group while studying the skew scattering of electrons and holes at an exchange-split interface or a spin-orbit tunneling barrier separating the two GaMnAs layers. Accordingly, carriers with opposite in-plane wave vector directions undergo asymmetric transmission while passing through such structures, resulting in the appearance of a net charge current along the structure surface. ATHE has been shown to be an extraordinary phenomenon by its large magnitude, chirality, and universal nature. Various calculation methods, including perturbation and non-perturbation Green function methods as well as advanced numerical computations based on k.p formalism [13–15], have highlighted this fact. TAHE/ATHE has recently been discovered in new material groups [16, 17], showing its important implications for future research in the field of spinorbitronics.

In previous studies, ATHE was examined under the assumption that the systems are in anti-parallel (AP) configuration, with the magnetization of two GaMnAs layers having equal magnitudes but opposite directions. In this work, we investigate the effect in general cases where the magnetization vectors of the two electrodes are noncollinear and their magnitudes are different. We consider the off-normal tunneling of valence band holes through a semiconductor magnetic tunnel junction (MTJ) made of GaMnAs/GaAs/GaMnAs. The magnetization vector of the left electrode is fixed, whereas that of the right electrode can be changed. We investigate the transmission asymmetry as a function of both the magnetization magnitude at the right electrode and the angles between two magnetization vectors.

2. Problem description and the Hamiltonian

Here, we consider a magnetic tunnel junction (MTJ) composed of GaAs and GaMnAs grown along the $z = [001]$ crystalline axis, as shown in Fig. 1. This structure consists of an intrinsic GaAs semiconductor layer with thickness d acting as a tunneling barrier, sandwiched between two GaMnAs layers, one on the left (fixed) and the other on the right (free), acting as electrodes. $\vec{M}^{(L)}$ and $\vec{M}^{(R)}$ represent magnetization vectors at the left and right electrodes,

respectively. $\vec{M}^{(L,R)} = M^{(L,R)}\vec{m}^{(L,R)}$ where $M^{(L,R)}$ is the magnetization magnitudes and $\vec{m}^{(L,R)}$ is the unit vectors determining the direction of magnetizations. The system is not under the influence of any external electric or magnetic fields.

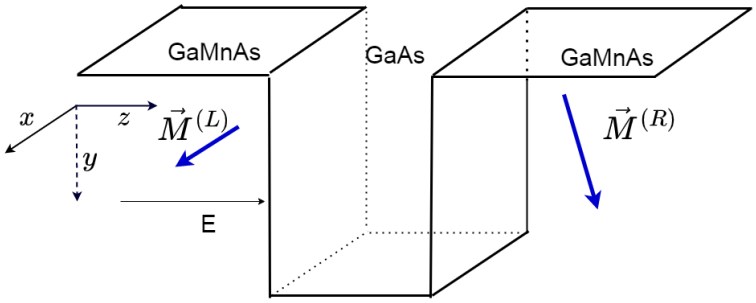

Fig. 1. Semiconductor MTJ in arbitrary configuration with unequal and noncollinear magnetization vectors at the two electrodes.

Considering off-normal tunneling of holes with kinetic energy E through the structure, the Schrodinger equation for the wave function is:

$$\left[H_0^{(j)} + H_{exc}^{(j)} + V^{(j)}\right]\Psi^{(j)} = E\Psi^{(j)}, \tag{1}$$

where $j = \{L,B,R\}$ stands for left electrode, barrier and right electrode correspondingly. $H_0^{(j)}$ is the Hamiltonian of the holes in intrinsic GaAs, $H_{exc}^{(j)}$ stands for the exchange Hamiltonian in GaMnAs, and $V^{(L)} = V^{(R)} = 0$ and $V^{(B)} = V_b$ are the potentials. Using six-band $k.p$ formalism, the Luttinger-Kohn Hamiltonian describing valence band holes is given by [18]:

$$H_0^{(j)} = \begin{pmatrix} -\gamma_1\check{k}^2 + \mathfrak{U} & \mathfrak{B} & \mathfrak{C} & 0 & \frac{1}{\sqrt{2}}\mathfrak{B}_\Delta & \sqrt{2}\mathfrak{C}_\Delta \\ cc & -\gamma_1\check{k}^2 - \mathfrak{U} & 0 & \mathfrak{C} & -\sqrt{2}\mathfrak{U}_\Delta & -\sqrt{\frac{3}{2}}\mathfrak{B}_\Delta \\ cc & cc & -\gamma_1\check{k}^2 - \mathfrak{U} & -\mathfrak{B} & -\sqrt{\frac{3}{2}}\mathfrak{B}_\Delta^* & \sqrt{2}\mathfrak{U}_\Delta \\ cc & cc & cc & -\gamma_1\check{k}^2 + \mathfrak{U} & -\sqrt{2}\mathfrak{C}_\Delta^* & \frac{1}{\sqrt{2}}\mathfrak{B}_\Delta^* \\ cc & cc & cc & cc & -\Delta - \gamma_{\Delta 1}\check{k}^2 & 0 \\ cc & cc & cc & cc & cc & -\Delta - \gamma_{\Delta 1}\check{k}^2 \end{pmatrix}. \tag{2}$$

We have chosen the energy origin at the top of the valence band and used the notations

$$\mathfrak{U} = \gamma_2(3\check{k}_z^2 - \check{k}^2),\ \ \mathfrak{B} = 2\sqrt{3}\gamma_3\check{k}_z(\check{k}_x - i\check{k}_y),\ \ \mathfrak{C} = \sqrt{3}\left[\gamma_2(\check{k}_x^2 - \check{k}_y^2 - 2i\gamma_3\check{k}_x\check{k}_y)\right];$$
$$\mathfrak{U}_\Delta = \gamma_{2\Delta}(3\check{k}_z^2 - \check{k}^2),\ \ \mathfrak{B}_\Delta = 2\sqrt{3}\gamma_{3\Delta}\check{k}_z(\check{k}_x - i\check{k}_y),\ \ \mathfrak{C}_\Delta = \sqrt{3}\left[\gamma_{2\Delta}(\check{k}_x^2 - \check{k}_y^2 - 2i\gamma_{3\Delta}\check{k}_x\check{k}_y)\right];$$

where $\check{k} = \hbar k^{(j)}/\sqrt{2m_0}$, m_0 is the mass of free electrons, and $k^{(j)} = [k_x^{(j)}, k_y^{(j)}, k_z^{(j)}]$ is the wave vector. The term $H_{exc}^{(j)}$ represents the $p-d$ exchange interaction between Mn magnetic impurities and GaAs. For the intrinsic GaAs in the barrier, we have $H_{exc}^{(B)} = 0$. For GaMnAs in the left and right electrodes, using the Zener mean-field model [19], $H_{exc}^{(L,R)}$ can be written as

$$\hat{H}_{\text{exc}}^{(L,R)} = \omega^{(L,R)}\vec{s}.\vec{m}^{(L,R)}. \tag{3}$$

In this formula, $\vec{s}$ is the spin operator written in Hamiltonian basis and $\omega^{(L,R)}$ is the exchange interaction strength that is proportinonal to the magnetization magnitude $M^{(L,R)}$ by $\omega^{(L,R)} = \frac{\beta M^{(L,R)}}{g\mu_B}$, where β is the exchange integral, g is the Landé coefficient, and μ_B is the Bohr magneton. The expressions for $\vec{s}$ and $\hat{H}_{\rm exc}$ have been represented in the Refs. [20,21].

3. Calculation Method

Choosing $z = 0$ at the interface between the barrier and the left electrode, we find the wave function in the jth region as

$$\Psi^{(j)} = e^{ik_\parallel \rho} \sum_{m=1}^{N=6} a_m^{(j)} \Phi_m(k_m^{(j)}) \exp(ik_m^{(j)}(z - z_0^{(j)})) + b_m^{(j)} \Phi_m(-k_m^{(j)}) \exp(-ik_m^{(j)}(z - z_0^{(j)})). \quad (4)$$

Here $z_0^{(L,B)} = 0$ and $z_0^{(R)} = a$; $k_\parallel$ is the in-plane wave vector component which is conserved during the tunneling process, and $k_m^{(j)}$ is the value of the component $k_z^{(j)}$, being the mth eigenvalue of the following eigenvalue equation

$$\det \| H_0^{(j)} + H_{exc}^{(j)} + V^{(j)} - E) \| = 0, \quad (5)$$

and $\Phi_m^{(j)}$ are the corresponding eigenvector. Note that normally Eq. (5) has $2N$ solutions. Due to time inversion symmetry, both $k_m^{(j)}$ and $-k_m^{(j)}$ are solutions. Therefore, in Eq. (4), we have arranged the waves propagating in the negative and positive directions separately, and used the notation $-k_m^{(j)} \equiv k_{m+N}^{(j)}$. Defining the current density operator in each region $\hat{J}_z^{(j)} = \partial \hat{H^{(j)}} / \partial p_z^{(j)} \equiv i \partial \hat{H^{(j)}} / \partial k_z$ ($\hbar = 1$), we have:

$$J_z^{(j)} \Psi^{(j)} = e^{ik_\parallel \rho} \sum_{m=1}^{N=6} a_m^{(j)} \left[J_z^{(j)} \exp(ik_m^{(j)}(z - z_0^{(j)})) \right] \Phi_m(k_m^{(j)}) + b_m^{(j)} \left[J_z^{j} \exp(-ik_m^{(j)}(z - z_0^{(j)})) \right] \Phi_m(-k_m^{(j)}). \quad (6)$$

Note that the Hamiltonian in Eq. (1) includes terms up to the second order of $k_z^{(j)}$. Expanding the Hamiltonian as Taylor series on $k_z^{(j)}$ yields

$$\begin{aligned} J_z^{(j)} \Psi^{(j)} &= e^{ik_\parallel \rho} \sum_{m=1}^{N=6} \Big\{ a_m^{(j)} \left[J^{(j)}(k_m) \Phi_m(k_m^{(j)}) \right] \exp(ik_m^{(j)}(z - z_0^{(j)})) \\ &\quad + b_m^{(j)} \left[J^{(j)}(-k_m) \Phi_m(-k_m^{(j)}) \right] \exp(-ik_m^{(j)}(z - z_0^{(j)})) \Big\} \quad (7) \\ &\equiv e^{ik_\parallel \rho} \sum_{m=1}^{N=6} a_m^{(j)} [J\Phi]_m(k_m^{(j)}) \exp(ik_m^{(j)}(z - z_0^{(j)})) + b_m^{(j)} [J\Phi]_m(-k_m^{(j)}) \exp(-ik_m^{(j)}(z - z_0^{(j)})) \end{aligned}$$

Here $J^{(j)}(k_m^{(j)}) = i \frac{\partial H^j}{\partial k_z} \big|_{k_z = k_m^{(j)}}$ is the current density calculated at $k_z^{(j)} = k_m^{(j)}$. Note also that the eigenvector $\Phi_m(k_m^{(j)})$ is an N- element column vector, and $J^{(j)}(k_m^{(j)})$ is a $N \times N$ matrix, therefore $[J\Phi]_m(k_m^j) = J^j(k_m)\Phi_m(k_m^{(j)})$ is also an N- element column vector. Using the $2N \times 2N$ matrix which is constituted from the set of $\Phi_m(k_m^{(j)})$ and $[J\Phi]_m(k_m^{(j)})$, we can combine Eqs. (4,6) in a convenient form:

$$\begin{bmatrix} \Psi^j(z) \\ J_z\Psi^j(z) \end{bmatrix} = \begin{bmatrix} \Phi_{1,1}(k_1^{(j)}) & \dots & \Phi_{1,2N}(k_{2N}^{(j)}) \\ \cdot & \cdot & \cdot \\ \cdot & \cdot & \cdot \\ \Phi_{N,1}(k_1^{(j)}) & \dots & \Phi_{N,2N}(k_{2N}^{(j)}) \\ [J\Phi]_{1,1}(k_1^{(j)}) & \dots & [J\Phi]_{1,2N}(k_{2N}^{(j)}) \\ \cdot & \cdot & \cdot \\ \cdot & \cdot & \cdot \\ [J\Phi]_{N,1}(k_1^{(j)}) & \dots & [J\Phi]_{N,2N}(k_{2N}^{(j)}) \end{bmatrix} \begin{bmatrix} e^{k_1^{(j)}(z-z_0^{(j)})} & \dots & 0 \\ \cdot & \cdot & \cdot \\ \cdot & \cdot & \cdot \\ \cdot & \cdot & \cdot \\ \cdot & \cdot & \cdot \\ \cdot & \cdot & \cdot \\ \cdot & \cdot & \cdot \\ 0 & \dots & e^{k_{2N}^{(j)}(z-z_0^{(j)})} \end{bmatrix} \begin{bmatrix} a_1^{(j)} \\ \cdot \\ \cdot \\ a_N^{(j)} \\ b_1^{(j)} \\ \cdot \\ \cdot \\ b_N^{(j)} \end{bmatrix}. \quad (8)$$

The boundary conditions that $\Psi_z^{(j)}$ and $J_z^{(j)}\Psi_z^{(j)}$ are continuous at $z = 0$ and $z = a$ give us:

$$\begin{bmatrix} a_1^{(L)} \\ \cdot \\ \cdot \\ a_N^{(L)} \\ b_1^{(L)} \\ \cdot \\ \cdot \\ b_N^{(L)} \end{bmatrix} = T \begin{bmatrix} a_1^{(R)} \\ \cdot \\ \cdot \\ a_N^{(R)} \\ b_1^{(R)} \\ \cdot \\ \cdot \\ b_N^{(R)} \end{bmatrix} \quad (9)$$

in which

$$T = IM(0)Q_B^{-1}IM(a) \quad (10)$$

where

$$IM(0) = \begin{bmatrix} \Phi_{1,1}(k_1^{(L)}) & \dots & \Phi_{1,2N}(k_{2N}^{(L)}) \\ \cdot & \cdot & \cdot \\ \cdot & \cdot & \cdot \\ \Phi_{N,1}(k_1^{(L)}) & \dots & \Phi_{N,2N}(k_{2N}^{(L)}) \\ [J\Phi]_{1,1}(k_1^{(L)}) & \dots & [J\Phi]_{1,2N}(k_{2N}^{(j)}) \\ \cdot & \cdot & \cdot \\ \cdot & \cdot & \cdot \\ [J\Phi]_{N,1}(k_1^{(L)}) & \dots & [J\Phi]_{N,2N}(k_{2N}^{(L)}) \end{bmatrix}^{-1} \begin{bmatrix} \Phi_{1,1}(k_1^{(B)}) & \dots & \Phi_{1,2N}(k_{2N}^{(B)}) \\ \cdot & \cdot & \cdot \\ \cdot & \cdot & \cdot \\ \Phi_{N,1}(k_1^{(B)}) & \dots & \Phi_{N,2N}(k_{2N}^{(B)}) \\ [J\Phi]_{1,1}(k_1^{(B)}) & \dots & [J\Phi]_{1,2N}(k_{2N}^{(B)}) \\ \cdot & \cdot & \cdot \\ \cdot & \cdot & \cdot \\ [J\Phi]_{N,1}(k_1^{(B)}) & \dots & [J\Phi]_{N,2N}(k_{2N}^{(B)}) \end{bmatrix}, \quad (11)$$

and

$$IM(a) = \begin{bmatrix} \Phi_{1,1}(k_1^{(B)}) & \dots & \Phi_{1,2N}(k_{2N}^{(B)}) \\ \cdot & \cdot & \cdot \\ \cdot & \cdot & \cdot \\ \Phi_{N,1}(k_1^{(B)}) & \dots & \Phi_{N,2N}(k_{2N}^{(B)}) \\ [J\Phi]_{1,1}(k_1^{(B)}) & \dots & [J\Phi]_{1,2N}(k_{2N}^{(B)}) \\ \cdot & \cdot & \cdot \\ \cdot & \cdot & \cdot \\ [J\Phi]_{N,1}(k_1^{(B)}) & \dots & [J\Phi]_{N,2N}(k_{2N}^{(B)}) \end{bmatrix}^{-1} \begin{bmatrix} \Phi_{1,1}(k_1^{(R)}) & \dots & \Phi_{1,2N}(k_{2N}^{(R)}) \\ \cdot & \cdot & \cdot \\ \cdot & \cdot & \cdot \\ \Phi_{N,1}(k_1^{(R)}) & \dots & \Phi_{N,2N}(k_{2N}^{(R)}) \\ [J\Phi]_{1,1}(k_1^{(R)}) & \dots & [J\Phi]_{1,2N}(k_{2N}^{(R)}) \\ \cdot & \cdot & \cdot \\ \cdot & \cdot & \cdot \\ [J\Phi]_{N,1}(k_1^{(R)}) & \dots & [J\Phi]_{N,2N}(k_{2N}^{(R)}) \end{bmatrix} \quad (12)$$

are the so-called interface matrices, and

$$Q = \begin{bmatrix} e^{k_1^{(B)}a} & \dots & 0 \\ . & . & . \\ . & . & . \\ . & . & . \\ . & . & . \\ . & . & . \\ . & . & . \\ 0 & \dots & e^{k_{2N}^{(B)}a} \end{bmatrix} \tag{13}$$

is the matrix representing the phase propagation in the barrier. T is the so-called transmission matrix relating the left electrode's wave amplitude to the right electrode's wave amplitude. Note that here T is a $2N \times 2N$ matrix. T in terms of two $N \times N$ matrices t and r is rewritten as follows:

$$T = \begin{bmatrix} t^{-1} & -t^{-1}r' \\ rt^{-1} & t' - rt^{-1}r' \end{bmatrix}. \tag{14}$$

The total transmission coefficient is calculated by $\mathscr{T} = \mathrm{Tr}\, t^{\dagger}t$. After obtaining the transmission coefficients, we can calculate the transmission asymmetry characterized for the ATHE as:

$$\mathscr{A} = \frac{\mathscr{T}_{k_\parallel} - \mathscr{T}_{-k_\parallel}}{\mathscr{T}_{k_\parallel} + \mathscr{T}_{-k_\parallel}}. \tag{15}$$

4. Result and Diccussion

The Luttinger parameters of the Hamiltonian in Eq. (3) are chosen as $\gamma_1 = 6.85$, $\gamma_2 = 2.1$, $\gamma_3 = 2.9$. These parameters provide hole masses from the 6×6 **k.p** matrix consistent with the experimental data [22]. The spin split-off energy value $\Delta = 0.31$ eV from Schottky barrier electroreflectance measurements is taken into account. In GaAs, Δ is much smaller than the bandgap energy; therefore, the approximation $\gamma_{\Delta 1} \approx \gamma_1$, $\gamma_{\Delta 2} \approx \gamma_2$, and $\gamma_{\Delta 3} \approx \gamma_3$ can be applied [18]. The barrier thickness is $d = 3$ nm and the potential height is $V_b = -0.6$ eV. The magnetization of the left electrode is along the x direction, i.e., $\vec{m}^{(L)} = [1,\ 0,\ 0]$, and its magnitude is constant with respect to $\omega^{(L)} = 0.15$ eV. The valence band holes are injected into the structure with an in-plane wave vector component $k_\parallel = [0.02,\ 0.02]$ Å^{-1}. The band structure of the left GaMnAs layer is shown in Fig. 2, where the top of the spin subbands $HH_\uparrow$, $HL_\uparrow$, $HL_\downarrow$, $HH_\downarrow$, $SO_\uparrow$, and $SO_\downarrow$ are located in descending order of energy levels.

We will first examine the effect of the magnitude of the right electrode's magnetization on the transmission asymmetry. To do this, we consider the system in an anti-parallel (AP)-like configuration, where the magnetization directions of the two electrodes remain opposite (i.e., $m^{(R)} = [-1,0,0]$), but their magnitudes are not equal (i.e., $\omega^{(R)} \neq \omega^{(L)}$). To obtain the complete picture of the system's properties, for a specified value of $\omega^{(R)}$, we calculate the asymmetry within a tunneling energy range that covers all valence spin subbands.

The transmission asymmetry as a function of tunneling energy for $\omega^{(R)} = 0.05$ eV (dashed line), $\omega^{(R)} = 0.1$ eV (dotted line), $\omega^{(R)} = 0.15$ eV (solid line), and $\omega^{(R)} = 0.2$ eV (dotted dashed line) are shown in Fig.3. The solid line corresponding to the antiparallel case ($\omega^{(R)} = \omega^{(L)} = 0.15$ eV) [12] is considered as a reference line. Interestingly, all the curves exhibit the same behavior.

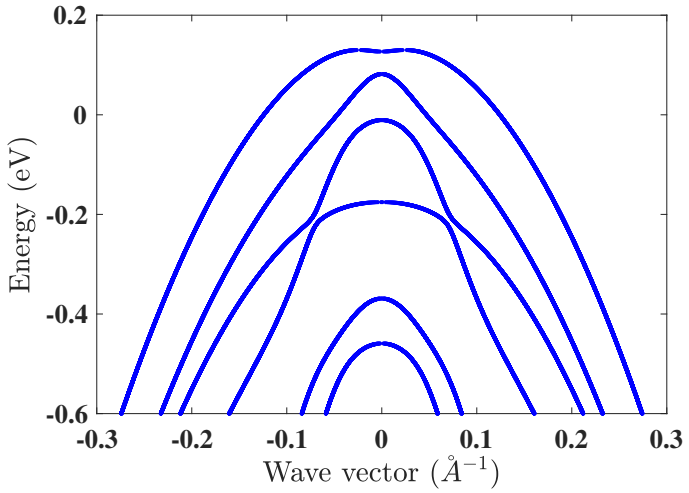

Fig. 2. Band structure of the holes in GaMnAs electrode. From top to bottom are the spin subbands $HH_{\uparrow}^{(L)}, HL_{\uparrow}^{(L)}, HL_{\downarrow}^{(L)}, HH_{\downarrow}^{(L)}, SO_{\uparrow}^{(L)}$, and $SO_{\downarrow}^{(L)}$.

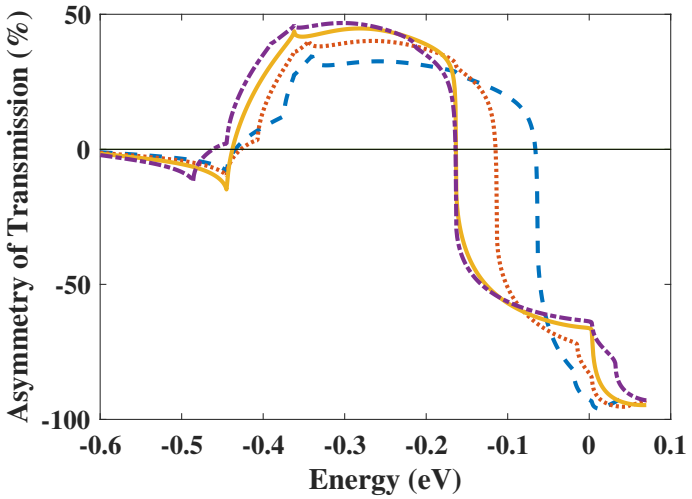

Fig. 3. Transmission asymmetry *vs* tunneling energy for different values of right electrode exchange energy: $\omega^{(R)} = 0.05$ eV (dashed line), $\omega^{(R)} = 0.1$ eV (dotted line), $\omega^{(R)} = 0.15$ eV (solid line) [12], and $\omega^{(R)} = 0.2$ eV (dash-dotted line).

The transmission asymmetry $\mathscr{A}$ crosses the zero value twice and changes its sign from negative to positive and *vice versa*. In increasing $\omega^{(R)}$, the curves are shifted towards the lower-energy regime and then asymptote to the reference line when $\omega^{(R)}$ reaches $\omega^{(L)}$. This saturation characteristics persists even for $\omega^{(R)} > \omega^{L}$. We also observe that changes in the magnitudes of $\omega^{(R)}$ have little influence on the asymmetry in the $E > 0$ region, where only $HH_{\uparrow}$ and $LH_{\uparrow}$ subbands contribute to the tunneling process. Similarly, in the $E < -0.45$ eV region, where all spin subbands participate

in tunneling, the effect of $\omega^{(R)}$ on asymmetry is also negligible. The effect of $\omega^{(R)}$ becomes apparent when the tunneling energy is between -0.4 and 0 eV. In particular, in the vicinity of $E = -0.1$ eV both the magnitude and sign of $\mathscr{A}$ strongly depend on the value of $\omega^{(R)}$. Therefore, we predict that the magnetization magnitude determines the tunneling properties of the down-spin light hole. Additionally, the dependence of the transmission asymmetry on the exchange energy for specific injection energies is shown in Fig. 4.

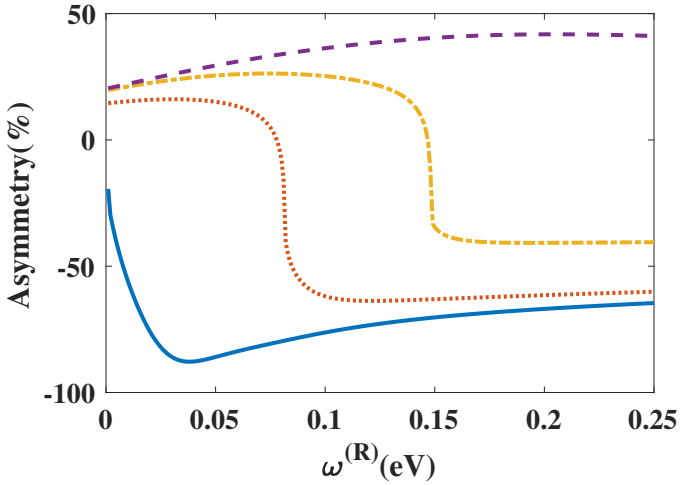

Fig. 4. The transmission asymmetry *vs* the right electrode exchange energy at specific injection energy values: $E = -0.035$ eV (solid line), $E = -0.1$ eV (dotted line), $E = -0.165$ eV (dash-dotted line), and $E = -0.3$ eV (dashed line).

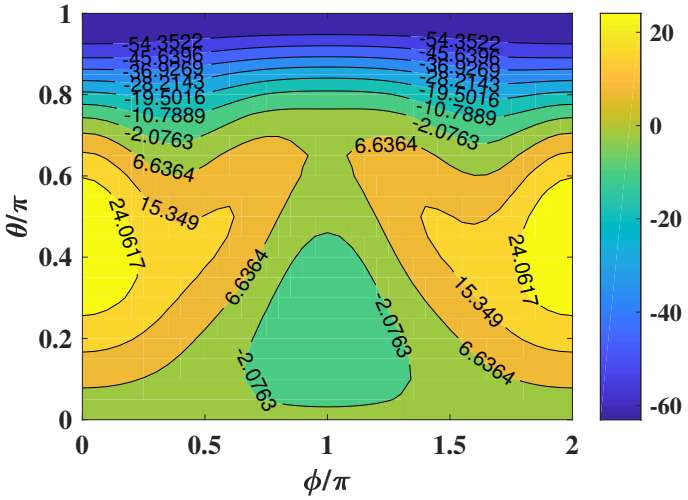

Fig. 5. Transmission asymmetry on (θ, ϕ) pannel. The $\mathscr{A}$ values are depicted by the corresponding colors as displayed in the color bar. Each contour line presents a constant asymmetry level.

Finally, we examine the transmission asymmetry when the system is in arbitrary magnetization configurations, where the magnetization vectors at the two electrodes are noncollinear. Because $\vec{m}^{(L)}$ is aligned with the x-axis, the position of $\vec{m}^{(R)}$ relative to $\vec{m}^{(L)}$ can be described through three components: $m_x^{(R)} = \cos\theta$, $m_y^{(R)} = \sin\theta\cos\phi$, and $m_z^{(R)} = \sin\theta\sin\phi$, where $\theta \in [0,\pi]$ represents the polar angle, and $\phi \in [0,2\pi]$ represents the azimuthal angle with respect to the x-axis. Taking $\omega^{(R)} = \omega^{(L)} = 0.15$ eV and the tunneling energy $E = -0.1$ eV, we calculate the transmission asymmetry coefficient on varying (θ,ϕ).

Figure 5 shows the transmission asymmetry in (ϕ,θ) panel, where the asymmetry values are depicted by the corresponding colors as displayed in the color bar and each contour line presents a constant asymmetry level. As the system approaches the parallel configuration (PA) (i.e., when $\theta \approx 0$), the asymmetry parameter $\mathscr{A}$ becomes zero, which is consistent with intuition. Conversely, when the system approaches the anti-parallel configuration (AP), $\mathscr{A}$ exhibits significant negative values (up to 70%) and shows little variation with respect to ϕ. In the intermediate states, $\mathscr{A}$ reaches its maximum positive value of 30% when the system is close to the spin transfer state (ST) (yellow regions). Generally, the transmission asymmetry exhibits a strong dependence on θ, whereas its dependence on ϕ is relatively weak.

The relative positions of the two magnetization vectors in the electrodes can be varied in magnetization switching process. The spin current flowing in the structure induces spin torques that affect the magnetization vectors. Its dynamics is governed by the Landau– Liftshit–Gilbert–Slonczewski equation [6]. The polar angle θ and the azimuthal angle ϕ determing the precession of the magnetization vector on the right electrode around that on the left electrode are functions of time. From our calculation, $\mathscr{A} = \mathscr{A}(\theta,\phi) = \mathscr{A}(t)$, the time-dependent information of the ATHE current can be obtained, which complete picture of the dynamics of the magnetization switching process.

5. Conclusion

In this work, we have investigated the asymmetry of the hole tunneling in a semiconductor -based MTJ in an arbitrary configuration. Namely, the two magnetization vectors are different in either magnitude or direction. The results show that the transmission asymmetry depends strongly on the magnitude of the right magnetization, particularly in the tunneling energy region where the down-spin light hole involves. Moreover, the asymmetry coefficient depends on the polar angle θ more than on the azimuthal angle ϕ between the two magnetization vectors. The result of this work motivates us to study the dynamics of anomalous tunneling hall current during magnetization switching process in the future.

Acknowledgment

Hoai. T. L. Nguyen would like to acknowledge the International Center of Physics for support of this research (Grant No. ICP.2022.12).

References

[1] B. Engel, J. Akerman, B. Butcher, R. Dave, M. DeHerrera, M. Durlam *et al.*, *A 4-mb toggle mram based on a novel bit and switching method*, IEEE Trans. Magn. **41** (2005) 132.

[2] Everspin Technologies Inc, "Spin-transfer torque DDR products." https://www.everspin.com/spin-transfer-torque-mram-products, 2020.

[3] M. N. Baibich, J. M. Broto, A. Fert, F. N. Van Dau, F. Petroff, P. Etienne *et al.*, *Giant magnetoresistance of (001) Fe/(001) Cr magnetic superlattices*, Phys. Rev. Lett. **61** (1988) 2472.
[4] G. Binasch, P. Grünberg, F. Saurenbach and W. Zinn, *Enhanced magnetoresistance in layered magnetic structures with antiferromagnetic interlayer exchange*, Phys. Rev. B **39** (1989) 4828.
[5] M. Julliere, *Tunneling between ferromagnetic films*, Phys. Lett. A **54** (1975) 225.
[6] J. C. Slonczewski, *Current-driven excitation of magnetic multilayers*, J. Magn. Magn. Mater. **159** (1996) L1.
[7] J. Hirsch, *Spin hall effect*, Phys. Rev. Lett. **83** (1999) 1834.
[8] S. D. Ganichev, E. Ivchenko, V. Bel'Kov, S. Tarasenko, M. Sollinger, D. Weiss *et al.*, *Spin-galvanic effect*, Nature **417** (2002) 153.
[9] E. I. Rashba, *Spin currents in thermodynamic equilibrium: The challenge of discerning transport currents*, Phys. Rev. B **68** (2003) 241315.
[10] T. H. Nguyen, H.-J. Drouhin and G. Fishman, *Spin trajectory along an evanescent loop in zinc-blende semiconductors*, Physical Review B **80** (2009) 075207.
[11] A. Matos-Abiague and J. Fabian, *Tunneling anomalous and spin hall effects*, Phys. Rev. Lett. **115** (2015) 056602.
[12] T. H. Dang, H. Jaffrès, T. H. Nguyen and H.-J. Drouhin, *Giant forward-scattering asymmetry and anomalous tunnel hall effect at spin-orbit-split and exchange-split interfaces*, Phys. Rev. B **92** (2015) 060403.
[13] T. H. Dang, D. Q. To, E. Erina, T. H. Nguyen, V. Safarov, H. Jaffrès *et al.*, *Theory of the anomalous tunnel hall effect at ferromagnet-semiconductor junctions*, J. Magn. Magn. Mater. **459** (2018) 37.
[14] D. Q. To, T.-H. Dang, H. Nguyen, V. Safarov, J.-M. George, H.-J. Drouhin *et al.*, *Spin-orbit currents, spin-transfer torque and anomalous tunneling in iii–v heterostructures probed by advanced 30-and 40-bands $k \cdot p$ tunneling methods*, IEEE Trans. Magn. **55** (2019) 1.
[15] I. Rozhansky, D. Q. To, H. Jaffrès and H.-J. Drouhin, *Chirality-induced tunneling asymmetry at a semiconductor interface*, Phys. Rev. B **102** (2020) 045428.
[16] M. Y. Zhuravlev, A. Alexandrov, L. Tao and E. Y. Tsymbal, *Tunneling anomalous hall effect in a ferroelectric tunnel junction*, Appl. Phys. Lett. **113** (2018) .
[17] D.-F. Shao, S.-H. Zhang, R.-C. Xiao, Z.-A. Wang, W. J. Lu, Y. P. Sun *et al.*, *Spin-neutral tunneling anomalous hall effect*, Phys. Rev. B **106** (2022) L180404.
[18] G. Fishman, *Semi-conducteurs: les bases de la théorie kp*. Editions Ecole Polytechnique, 2010.
[19] T. Dietl, o. H. Ohno and F. Matsukura, *Hole-mediated ferromagnetism in tetrahedrally coordinated semiconductors*, Phys. Rev. B **63** (2001) 195205.
[20] T. H. Nguyen, H.-J. Drouhin and G. Fishman, *Spin trajectory along an evanescent loop in zinc-blende semiconductors*, Phys. Rev. B **80** (2009) 075207.
[21] D.-Q. To, *Advanced kp multiband methods for semiconductor-based spinorbitronics*, Ph.D. thesis, Institut polytechnique de Paris, 2019.
[22] M. Lantz, H. Hug, R. Hoffmann, S. Martin, A. Baratoff and H.-J. Güntherodt, *Short-range electrostatic interactions in atomic-resolution scanning force microscopy on the si (111) 7× 7 surface*, Phys. Rev. B **68** (2003) 035324.